DE GRUYTER OPEN

Journal of ELECTRICAL ENGINEERING, VOL 68 (2017), NO1, 23–30

Analysis and identification of influential phenomena on iron losses in embedded permanent magnet synchronous machine

Mitja Breznik, [*] **Viktor Goričan,** [**] **Anton Hamler,** [**] **Selma Čorović,** [***] **Damijan Miljavec** [***]

This paper presents magnetic flux density behaviour in laminated electrical sheets which affects the results and precision of iron losses calculation in imbedded permanent magnet (IPM) machine. Objective of the research was to analyse all the influential phenomena that were identified through iron loss models analysis, finite element method simulations and iron loss measurements. The presence of phenomena such as harmonic content and rotational magnetic fields are confirmed with finite element method analysis of concentrated and distributed winding IPM machine. A significant magnetic flux density ripple in the rotor of concentrated winding IPM machine in comparison to distributed winding IPM machine is revealed and analysed. Behaviour that affects iron loss in the rotor of synchronous machines in the absence of first order harmonic is analysed. The DC level added to alternating magnetic flux density was used in experiment to mimic magnetic behaviour on the rotor of IPM machine and further to calculate iron losses.

K e y w o r d s: iron losses, permanent magnet synchronous machine, rotational magnetic flux density, Bertotti model, loss surface model

1 Introduction

Permanent magnet synchronous machine has been used on a wide range of applications [1]. The shift to a more efficient and compact designs was encouraged by environmental awareness and low production cost. Iron loss presents a significant part of total losses in imbedded permanent magnet synchronous machine (IPM) that was chosen as a representative case to illustrate the approach. Importance of iron losses calculation has increased due to modern higher pole number designs that must reach a wide range of mechanical loads and rotational speeds [2]. Mentioned behaviour is most evident in electric vehicle drives [3, 4]. Prediction of iron losses and consequently prediction of efficiency, optimization procedures and thermal analysis can be done only by deep understanding of iron loss effects and study of magnetic behaviour in analysed machine. Use of commercial FEM software for synchronous machine analysis with a wide range of implemented tools shadows the actual mechanism of iron loss models and the theory behind it. In order to implement and analyse each step necessary for magnetic analysis and iron loss calculation a basic open source software with static FEM analysis is used.

2 Iron loss models

Iron loss resulting from a change in magnetization can be determined with many iron loss models. It has to be noted that electrical sheet steel cannot be represented as a homogenous structure in the study of magnetization mechanism. The magnetization process is localised on each magnetic domain that changes in size during magnetization process [5]. Iron loss models that are appropriate for analysis of electric machines are usually based on separation of iron losses into a form of static and dynamic behaviour stated as hysteresis, eddy current and excess losses [6]. When using models presented later in the article one has to recognise the simplification of loss separation and independent analysis on each finite element. The above-stated approach neglects the effect of nonhomogeneous eddy current distribution throughout the steel sheet and the impact of eddy currents on magnetic field distribution.

One of the models that were used in this study is Bertotti model [7]. Mentioned model is based on the separation of losses into three contributions:

$$p_{fe} = C_0 f \hat{B}^2 + \frac{\pi^2 \sigma d^2}{6} f^2 \hat{B}^2 + C_1 f^{(3/2)} \hat{B}^{3/2} \qquad (1)$$

where C_0 represents the hysteresis losses coefficient, d steel sheet thickness and C_1 value of excess losses coefficient. Apart from the coefficients determined from the used electrical steel, iron loss is influenced by the maximum value of magnetic flux density $\hat{B}$ in the analysed part of the ferromagnetic material and value of excitation frequency f.

Bertotti model can be further expanded so that the eddy and excess losses can be determined for an arbitrary

[*] Kolektor Group d.o.o., Idrija, Slovenia, [**] Faculty of Electrical Engineering and Computer Science, University of Maribor, Maribor, Slovenia, [***] Faculty of Electrical Engineering, University of Ljubljana, Ljubljana, Slovenia, damijan.niljavec.uni-lj.si

DOI: 10.1515/jee-2017-0003, Print (till 2015) ISSN 1335-3632, On-line ISSN 1339-309X

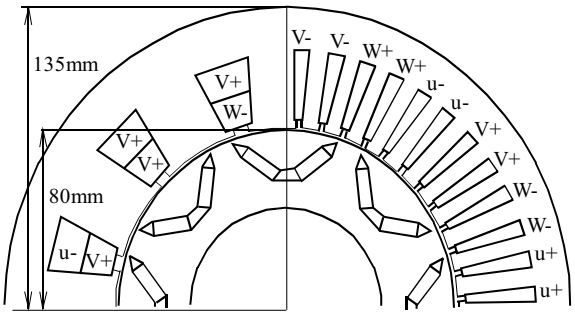

Fig. 1. Concentrated winding IPM machine (left) and distributed winding IPM machine (right) with the active length of 84 mm

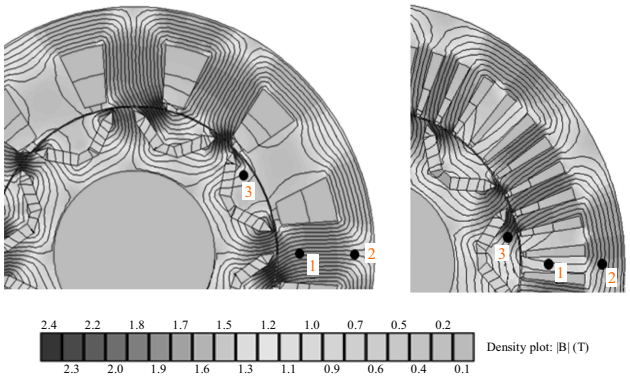

Fig. 2. Observation points for $\boldsymbol{B}(t,x,y)$ at (a) — concentrated winding and (b) — distributed winding machine

magnetic flux density waveform

$$p_{fe} = C_0 f \hat{B}^2 + \sigma \frac{\partial d^2}{\partial 12}\Big(\frac{\mathrm{d}B}{\mathrm{d}t}(t)\Big)^2 + k_e\Big(\Big|\frac{\mathrm{d}B}{\mathrm{d}t}(t)\Big|\Big)^{(3/2)} \quad (2)$$

Where k_e is excess losses coefficient for calculation using magnetic flux density derivative and σ represents electrical conductivity. Model based on equation (2) will be referred as modified Bertotti model. We can conclude that iron loss density is not only influenced by the maximum value of B but also by the harmonic content of waveform.

The influence of the magnetic flux density B harmonic content on iron loss density can also be observed with scalar dynamic hysteresis models such as Loss Surface (LS) model [8] (3). Model depends on determining magnetic field strength H from past time invariant changes of magnetic flux density $(B_n, B_{n-1}, \dots)$ that represent static contribution to magnetic field strength H_{stat} and dynamic contribution H_{dyn} modelled as dependence on magnetic flux density temporary value and its time derivative.

$$H = H_{\mathrm{stat}}(B_n, B_{n-1}, \dots) + H_{\mathrm{dyn}}\Big(B, \frac{\mathrm{d}B}{\mathrm{d}t}\Big). \quad (3)$$

Minor loops and widening of the hysteresis loop can be noticed when higher harmonics are present in the magnetic waveform which also affects iron loss value, Fig. 11.

Iron loss can also be modelled when magnetic quantities are regarded as vectors. Hysteresis loop is determined by reconstructing B and H with the vector hysteresis model [9]. Iron loss density is determined with the following equation (4) by the surface area of the hysteresis loop in x and y direction of electrical steel sheet. From the analysis of vector models we can conclude that the changing direction of magnetic flux density also affects iron loss value.

$$P.hyst = \frac{1}{T}\int_0^T \Big(H_x \frac{\mathrm{d}B_x}{\mathrm{d}t} + H_y \frac{\mathrm{d}B_y}{\mathrm{d}t}\Big)\mathrm{d}t\,. \quad (4)$$

3 Magnetic behaviour in IPM machine

For the purpose of magnetic behaviour analysis two IPM machines with "V" shape magnets were modelled. Machine geometry designs were based on synchronous machine that is used in a hybrid vehicle [10]. Both machines have identical rotor. BH curve of permanent magnets was modelled according to NdFeB N40 type. Magnetic properties of electrical steel resemble M400-50 steel grade. The stators are different in the type of used winding and number of stator slots. One machine has 12 stator slots and 8 rotor poles which is suitable for concentrated winding. Meanwhile, the other machine has 48 stator slots with distributed winding, Fig. 1. Both stators were modelled with identical stator slot area per-phase and teeth magnetic cross-section per-pole.

Transient analysis of maximum torque per ampere (MTPA) operating point for both machines was simulated using open source software [11]. Simulation consists of several magneto-static analyses in a time frame of one excitation period (3000 rpm, 141 Arms). Transient simulation of the operating point was achieved with a series of magneto-static simulations where rotor angle and phase current distribution was modified in each step to achieve sinusoidal current waveform and constant torque angle. Machine with distributed winding developed 304 Nm of torque with 8 % torque ripple. Machine with concentrated winding developed 254 Nm of torque with 21 % torque ripple.

3.1 Magnetic flux density depending on the observation point

Used FEM software enables access to physical quantities of each finite element. Method for spatial and time based observation of $\boldsymbol{B}$ was formed, which was noticed as influential in determining iron loss value. Points where magnetic flux density was observed are shown in Fig. 2.

Direction of $\boldsymbol{B}$ seen in the stator teeth of the distributed winding IPM does not change drastically, but the presence of higher harmonics is evident, Fig. 3. On the other hand rotation in the stator joke is significant, so occurrence of this phenomenon will be further identified. Magnetic flux density waveforms in the observation points on the stator did not reveal larger differences between both machines therefore, only the waveforms of the

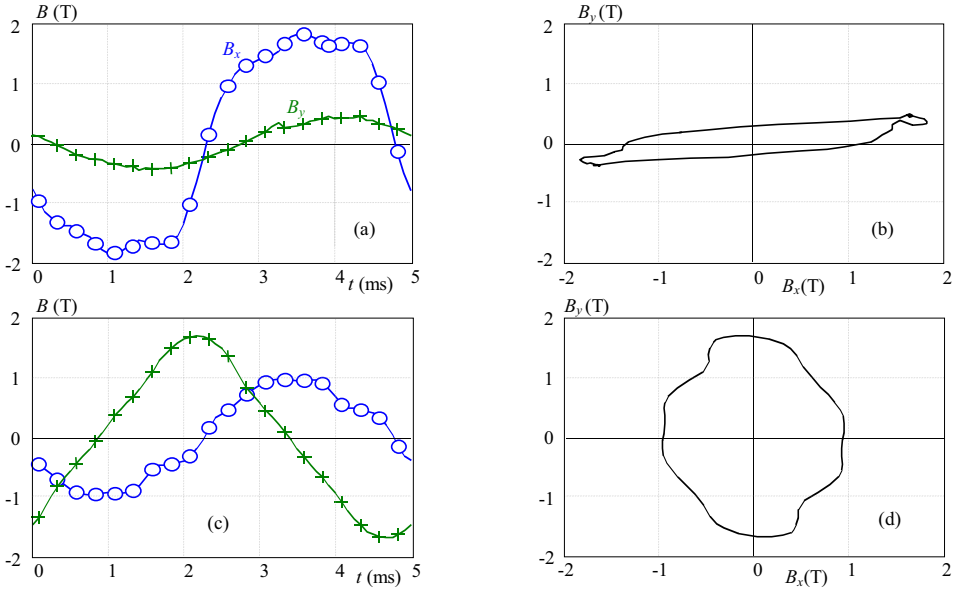

Fig. 3. Waveform of $B_x(t)$ and $B_y(t)$ in (a), (b) — the stator teeth (point 1) and (c), (d) — stator yoke of distributed winding machine (point 2)

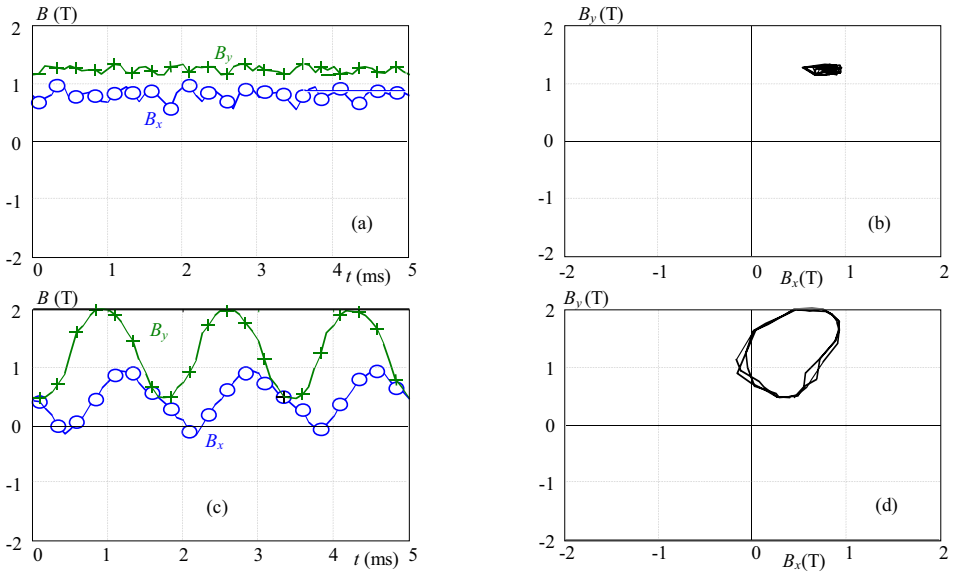

Fig. 4. Waveform of $B_x(t)$ and $B_y(t)$ in (a), (b) — the rotor of distributed winding IPM machine (point 3) and (c), (d) — the rotor of concentrated winding IPM machine (point 3)

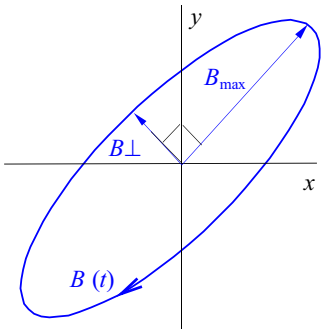

Fig. 5. Values of elliptical $\boldsymbol{B}(t)$ that are used to identify rotational magnetic fields

distributed winding IPM machine are shown. As expected DC component is present on the rotor of both machines, but we can see significant ripple of $\boldsymbol{B}$ in a machine with concentrated winding, Fig. 4.

3.2 Rotational magnetic fields in the stator

Identification procedure described below was developed to detect the extent and intensity of rotational magnetic fields in analysed machines. Rotation of magnetic field is a behaviour at which magnetic flux density in ferromagnetic material not only changes in size but also changes direction throughout the excitation period. The rotation is presented with the ratio of magnetic flux density in two directions $\boldsymbol{B}_\perp$ and $\boldsymbol{B}_{\max}$. The meaning of ratio $|\boldsymbol{B}_\perp|/|\boldsymbol{B}_{\max}|$ is explained in case of elliptical rotation in Fig. 5. With the information of surface area of each finite element we can observe the magnetic loading

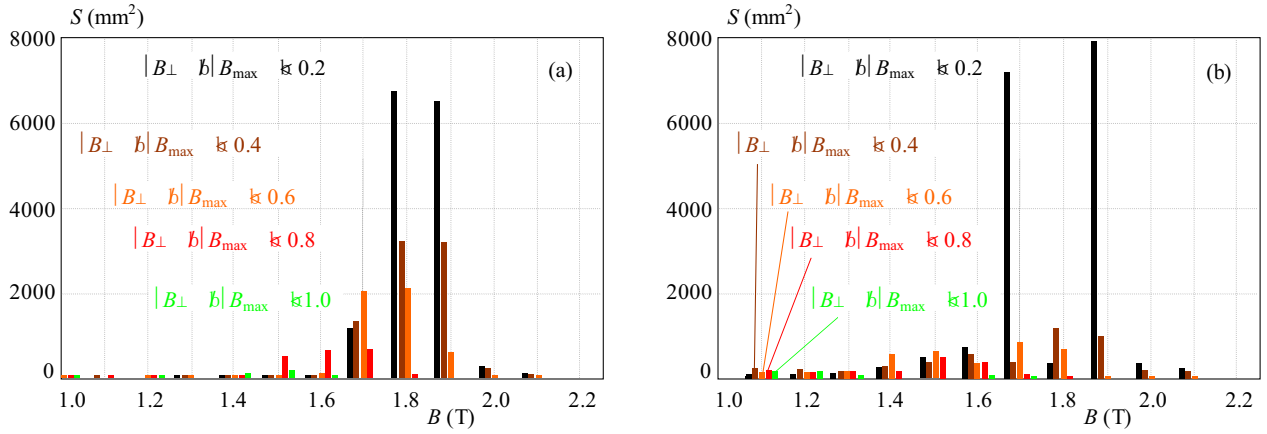

Fig. 6. The surface area S on stator depending on maximum value of B and ratio $|\boldsymbol{B}_\perp|/|\boldsymbol{B}_{\max}|$ in case of (a) — distributed winding and (b) — concentrated winding IPM machine

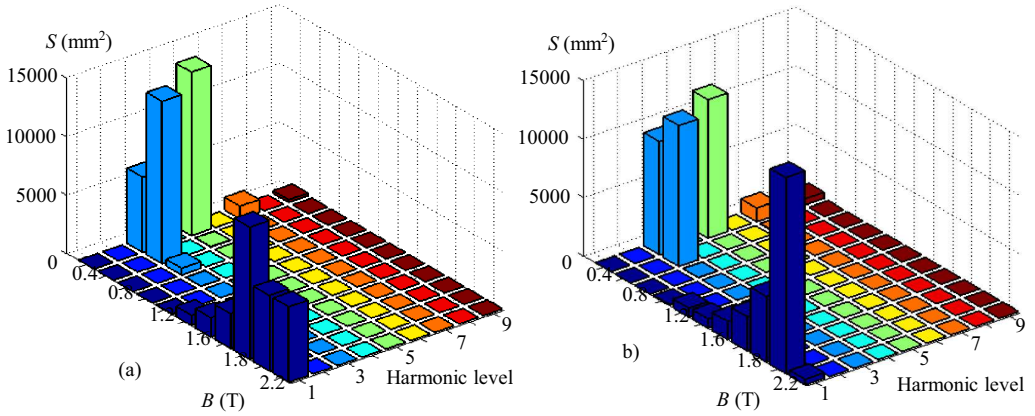

Fig. 7. Amount of surface area depending on harmonic order amplitude of B and harmonic level on stator of (a) — distributed and (b) — concentrated winding IPM machine

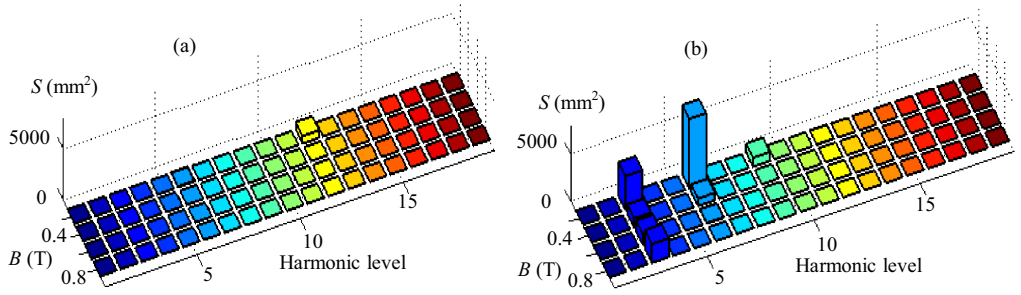

Fig. 8. Amount of surface area depending on harmonic order amplitude of B and harmonic level on rotor of (a) — distributed and (b) — concentrated winding IPM machine

depending on the maximum magnetic field density and the mentioned ratio. Information of the surface area that is exposed to a certain maximum value of B gives an insight into magnetic working point of the electrical sheet steel.

Figure 6 shows the surface area of the ferromagnetic material on the stator of analysed machines according to the maximum value of B and $|\boldsymbol{B}_\perp|/|\boldsymbol{B}_{\max}|$ ratio. Presence of rotational magnetic flux density is higher in distributed winding IPM machine especially in range of 1.7–1.9 T seen as a higher portion of surface area with higher $|\boldsymbol{B}_\perp|/|\boldsymbol{B}_{\max}|$ ratio, Fig. 6(a). Greater part of ferromagnetic material is exposed to high values of B (1.8–1.9 T) in case of distributed winding IPM machine Fig. 6(a) which could also contribute to higher calculated iron loss value.

3.3 Harmonic content of B waveform

Harmonic content of magnetic flux density in each finite element was analysed using Fourier transform. In Figures 7 and 8 surface area is shown in dependence on the harmonic order amplitude of magnetic flux density and harmonic level. As seen in Fig. 7 we can detect 3^{rd}, 5^{th} and 7^{th} harmonics on an extensive amount of surface area on the stator in case of both analysed machines. Used analysis is of significant importance for

Table 1. Values of measured iron loss density on RRSST sample in the case of added higher harmonics of different amplitude intensities and harmonic orders at $\hat{B} = 1.5$ T compared to predicted values by iron loss models

B wave -form	Measure--ment (W/kg)	Bertotti (%)	Modified Bertotti (%)	LS (%)
1st 50Hz	2.0	+12.9	+13.4	+5.9
+3rd, B_1	2.4	-7.5	+9.8	-3.3
+3rd, B_2	3.2	-28.2	+1.9	-0.3
+5th, B_1	2.2	+2.7	+14.9	+6.8
+5th, B_2	3.4	-33.9	+3.5	+2.9
+7th, B_1	2.9	-22.3	+4.5	+5.8
+7th, B_2	5.1	-55.2	-4.1	+9.1
1st 200 Hz	19.1	+1.0	+1.2	+2.3
+3rd, B_1	24.0	-19.6	+4.7	+1.0
+3rd, B_2	42.1	-54.1	-6.6	+5.7
+5th, B_1	22.6	-14.8	+1.4	+4.1
+5th, B_2	36.5	-47.2	+0.2	+7.7
+7th, B_1	27.6	-30.1	+0.2	+3.9
+7th, B_2	48.0	-60.0	+4.8	+15.3

$B_1 = 0.255$ T, $B_2 = 0.45$ T

analysing behaviour that affects iron loss on the rotor of synchronous machines in the absence of first order harmonic. As seen in Fig. 8 and mentioned in the previous section a harmonic content in the case of distributed winding machine is barely visible and just as the 12^{th} harmonic, Fig. 8(a). Whereas the presence of higher harmonics in case of concentrated winding machine is higher in amplitude and surface area, Fig. 8(b).

4 Iron loss measurements

When determining the value of iron loss of the electric machine it is important to understand the effects of technological processes such as punching, laser cutting and mechanical tension during manufacturing. Mentioned processes change the magnetic properties of the material in the close proximity of the performed mechanical process. Inferior magnetic properties in the mentioned area affect the whole magnetic distribution in the electric machine. If the manufacturing effects are neglected during the finite element analysis added measures must be taken to account for mentioned phenomena. With the approach presented below we can determine the effects of mentioned processes on iron loss value.

Samples of electrical steel sheets consist of two geometrically different laminated toroid shapes, Fig. 9(a) and one round rotational single sheet, Fig. 9(b). These samples enable directional scalar and rotational field iron loss measurements. For rotational field iron loss measurements round rotational single sheet tester (RRSST) [12] was used. Using RRSST tester the rotational as well as directional scalar field iron losses were measured on round single sheet sample.

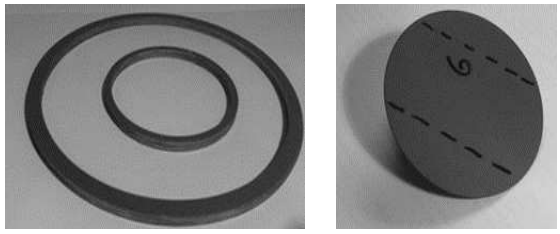

(a) (b)

Fig. 9. Toroid electrical steel samples: (a) — (160-145-6 and 80-73-6), (b) — RRSST sample with 78 mm in diameter

Measurements of iron loss at sinusoidal B waveform confirm the effect of mechanical processes on the iron loss. Iron loss density was higher up to 5 % in the case of smaller toroid sample due to the higher ratio of affected area with laser cutting process in comparison to the whole sample cross-section area. Iron loss density measured on RRSST sample differed between the rolling (0°) and transverse (90°) direction in case of nonoriented steel M400-50. Iron loss density measured on RRSST sample was lower (down-to 30 %) compared to the toroid samples since magnetic quantities on RRSST sample are measured on an area unaffected by technological processes. Anisotropic behaviour, mechanical stress during winding of toroid and effects of laser cutting contribute to higher iron loss value in toroid samples. All of above mentioned effects are more prominent at lower frequencies since they have a larger effect on static hysteresis losses, Fig. 10. At higher frequencies effects of manufacturing become less pronounced due to the prevailing eddy current losses. Differences between measurements caused by anisotropic properties and technological processes are an indication that great care must be taken when determining the coefficients of iron loss models.

The following measurements on RRSST sample confirm that harmonic content in B affects the iron loss. Waveform consisted of added 3^{rd}, 5^{th} and 7^{th} harmonics that were detected in FFT analysis, Fig. 7 at two different amplitude intensities. Loss density and hysteresis area, Fig. 11 increases with the amplitude and order of the added harmonic at the unaltered maximum B value.

Table 1 shows the accuracy of iron loss models at different magnetic flux density waveforms. Determination of the specific model parameters for the analysed steel sample is further explained in section 5. Classic Bertotti model is not suitable for heavily distorted B waveforms whereas modified Bertotti model and LS model both respond to harmonic content seen as consistent deviation in comparison to measured iron loss density, Table 1, with $B_1 = 0.255$ T, $B_2 = 0.450$ T resulting in $\hat{B} = 1.5$ T waveform.

Iron loss density in the case of elliptical $\boldsymbol{B}(t)$ waveform, Fig. 5, was measured on RRSST sample, with the same defined ratio that was used for rotational fields detection in IPM machine, Fig. 6. We can conclude that iron loss density increases with the increasing $|\boldsymbol{B}_\perp|/|\boldsymbol{B}_{\max}|$ ration. We can also spot a discrepancy in this statement at lower frequencies, Fig. 12, where the iron loss density

Table 2. Values of measured iron loss density in case of added magnetic flux density DC component compared to calculated values using iron loss models

B signal:			Measure -ment	Modified	LS Bertotti
DC	AC	f	(W/kg)	(%)	(%)
-	0.3	50	0.14	-50.0	-21.4
1.10	0.3	50	0.21	-66.0	+14.3
1.33	0.3	50	0.42	-83.0	+23.8
-	0.3	200	0.95	-17.9	-8.4
1.10	0.3	200	1.17	-33.3	+18.2
1.35	0.3	200	2.13	-63.4	+17.8
DC	AC	f		(W/kg)	(W/kg)
-	0.3	800	-	9.79	10.54
1.10	0.3	800	-	9.79	13.76
1.35	0.3	800	-	9.79	16.89

Table 3. Calculated values of iron loss with implemented iron loss models on the stator of analysed machines

Type of IPM winding	Bertotti (W)	Modified Bertotti (W)	LS - look up table (W)
Distributed	543	744	1046
Concentrated	501	722	1007

drops at higher magnetic flux densities and observed ratio due to a change in magnetization of magnetic domains under the influence of rotational magnetic fields. Magnetization vector under mentioned conditions rotates, whereas the proportions of magnetic domains do not change considerably. This phenomenon affects the iron loss determination with scalar models. In this article a procedure of superposition was used that can take into account rotation of magnetic quantities with scalar models. Rotational waveform was translated into two directions, as follows in the direction of $\boldsymbol{B}_{\max}$ and the direction of $\boldsymbol{B}_{\perp}$ [11]

$$p_{fe}\big(\boldsymbol{B}(t)\big) = p_{fe}\big(B_{\max}(t)\big) + p_{fe}\big(B_{\perp}(t)\big). \qquad (5)$$

Iron losses of each component were determined directly from the measurements in the case of sinusoidal scalar B waveform. It can be concluded, that the use of loss superposition is suitable for higher frequencies where eddy current losses are dominant Fig. 13. Since permanent magnet machine development aspires in the direction of higher pole pairs and excitation frequencies loss superposition can be used despite the inferior accuracy at lower frequencies.

Last experiment conducted on RRSST sample also mimics the magnetic behaviour on the rotor of IPM machine. Objective of this measurement was to determine how the DC level of B affects iron loss. Iron loss density and hysteresis area grew with the increasing DC level at the same AC component ($B_{\mathrm{AC}} = 0.3$ T), Fig. 14. Models that are based on the maximum value of waveform such as classic Bertotti model cannot be used, since they are tailored for alternating sinusoidal B waveforms. It can be seen that dynamic hysteresis models such as LS model responds to DC value of B. Meanwhile, the use of modified Bertotti model without hysteresis loss contribution is limited to higher frequencies where eddy currents dominate over hysteresis magnetization effects on iron loss, Table 2. As seen from the Fourier analysis of magnetic flux density waveform, Fig. 8, on the rotor of IPM machine higher excitation frequencies of B are expected, which can justify the usage of models that can determine the value of eddy current loss as predominant component of iron losses.

Table 4. Calculated values of iron loss with implemented iron loss models on the rotor of analysed machines

Type of IPM winding	Modified Bertotti (W)	LS - look up table (W)
Distributed	45	88
Concentrated	212	369

Table 5. Bertotti models coefficients of M400-50 electrical steel

C_0	σd^2	C_1	k_e
231.9	0.59	6.40	0.74

5 Iron loss calculation

Coefficients derived from measuring electrical steel M400-50 on RRSST sample in rolling direction were used to determine iron losses of two modelled IPM machines. Coefficients for Bertotti model were determined using surface fit method of Berttoti polynomic function (1) on measured data, Fig. 15 and Table 5. Parameters needed for LS model consisted of Tellinen static hysteresis measured at low excitation frequency for static hysteresis model [13] and coefficients determined from magnetic field strength measured at triangular flux density waveform, Fig. 16. Due to the application of models in post processing FEM analysis preliminary integration steps must be established. Vector type change of magnetic flux density waveform in each finite element was mapped in a direction of $\boldsymbol{B}_{\max}$, Fig. 5, to achieve a scalar change of magnetic flux density, since application of modified Bertotti model requires scalar magnetic flux density waveform (2). Involvement of LS model into FEM post processing environment was performed using loss superposition as suggested by research [14]. Instead of using static hysteresis model for static magnetic field strength H_{stat} calculation in case of LS model, magnetic field strength was determined straight from the measurement of H at triangular B waveforms. Magnetic field strength measured dependence in function of B and $\mathrm{d}B/\mathrm{d}t$ was then implemented using a look up table. Problems with convergence of static hysteresis models and functionality at high B values were avoided by applying upper described approach. Iron loss values correspond to the before presented working point (3000 rpm, 141 Arms).

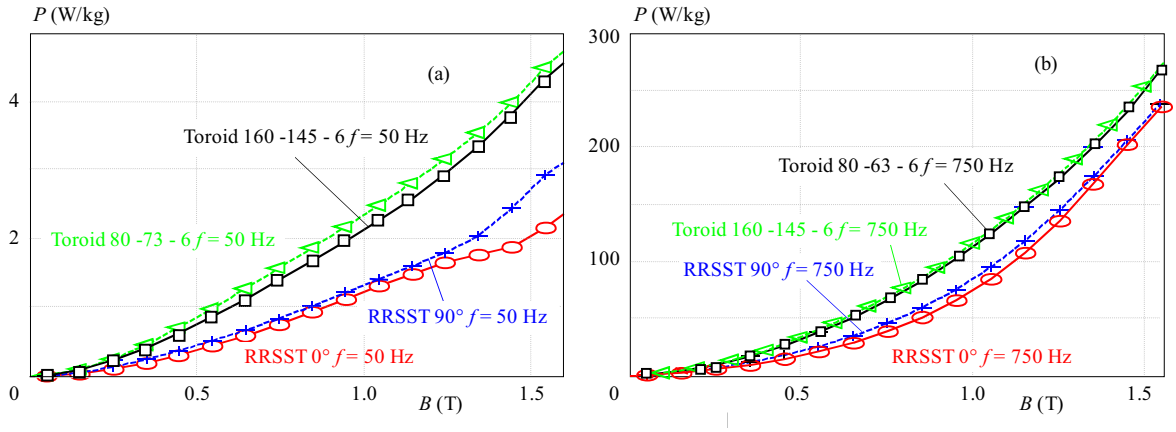

Fig. 10. Iron loss density in toroid and RRSST sample in rolling and transverse direction

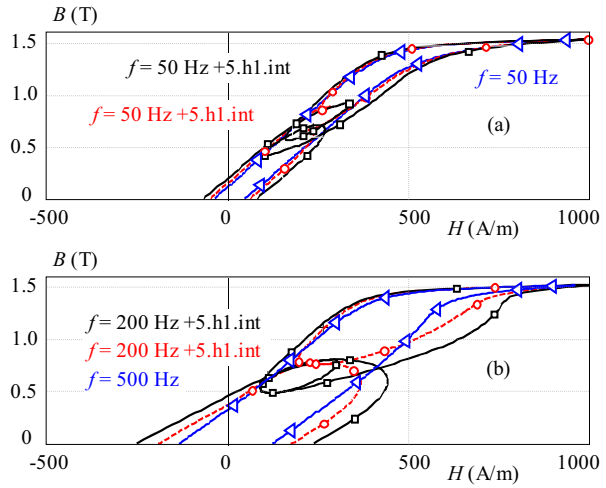

Fig. 11. Measured iron loss density in the case of elliptical waveforms at 200 Hz compared to calculated iron loss determined by using superposition

From the results, Table 3 we can see the increase in calculated losses with increasing complexity of used models, since more natural phenomena are considered and described. Losses in stator core of both machines are higher in the case of distributed winding IPM machine, Table 3, as predicted from magnetic loading analysis, Figs. 6 and 7. Losses on the rotor core of both machines are higher in the case of concentrated winding IPM machine, Table 4, as concluded from FFT study of B in each finite element and calculated losses in whole rotor, Table 4 and Fig. 8.

6 Conclusion

In this paper the effects of magnetic flux density harmonic content, rotation of magnetic quantities, presence of DC component in alternating magnetic flux density waveform and technological processes on iron losses were successfully analysed in case of IPM machine. Verification of iron loss models on steel samples was demonstrated for the later use in FEM design and simulation of rotating machines. Scalar models such as LS model were proven to be effective in determining iron loss value considering identified magnetic phenomena and were shown to be suitable for post processing integration. Study enables better understanding of effects that may cause the deviations of predicted and measured iron loss which way be beneficial in the design and prototyping phase of electric machines by applying the presented procedures to

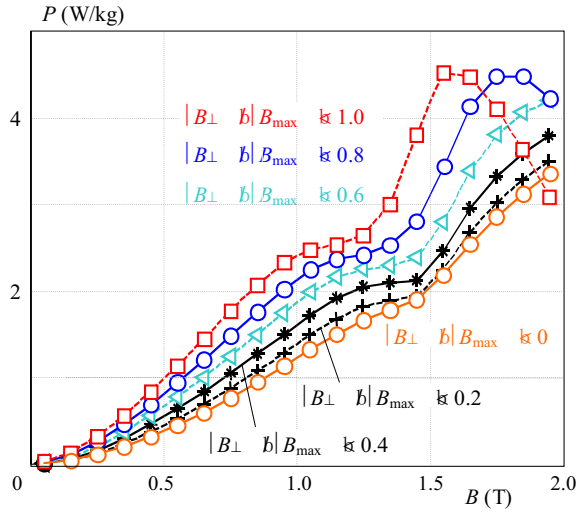

Fig. 12. Hysteresis loops with added DC component

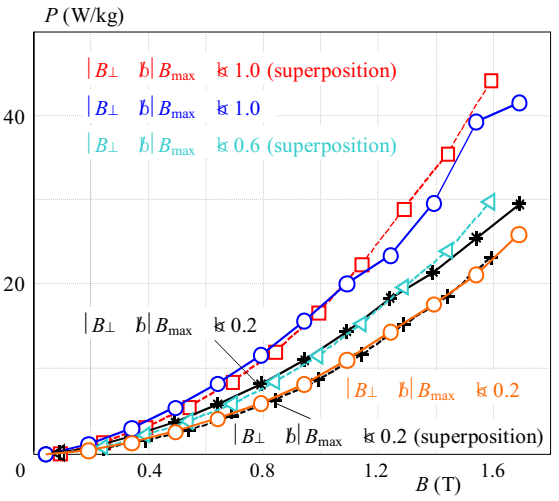

Fig. 13. Measured iron loss density in the case of elliptical waveforms at 200 Hz compared to calculated iron loss determined by using superposition

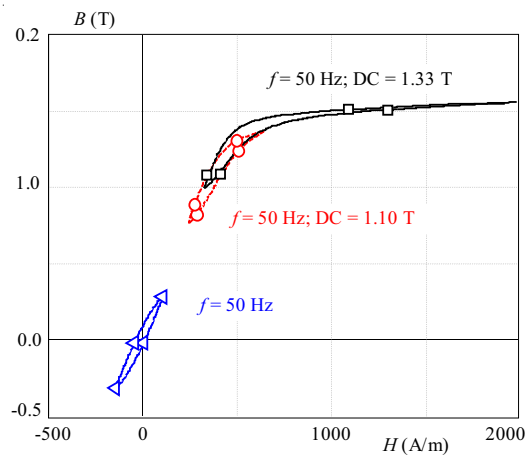

Fig. 14. Hysteresis loops with added DC component

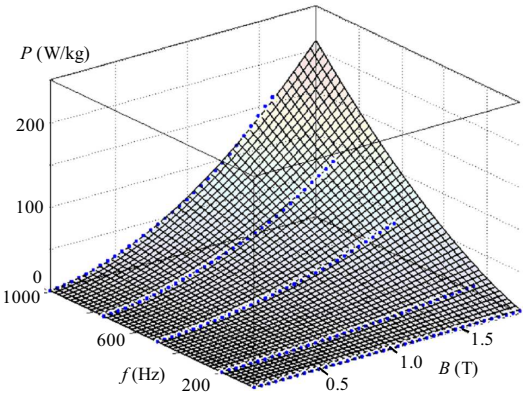

Fig. 15. Bertotti surface function (1) fitted on a measured iron loss density of M400-50 electrical steel

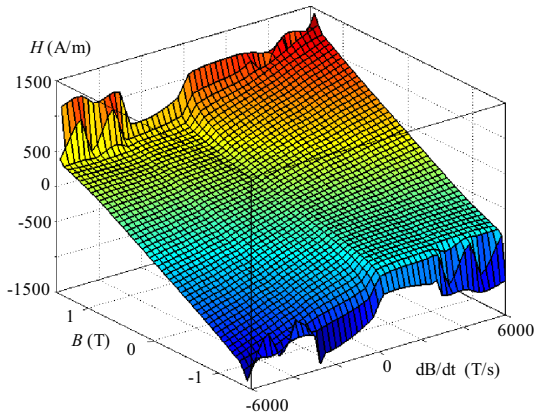

Fig. 16. Measured magnetic field strength at triangular magnetic flux density waveforms of M400-50 electrical steel

improve the development process. Implemented methodology was used to determine the value of iron losses in two different IPM machines that were used for the magnetic behaviour study. The study also reveals the higher level of iron losses in the rotor of concentrated winding IPM machine design. To avoid increased rotor temperature which can cause permanent magnet thermal partial or total demagnetization the use of distributed winding IPM machine design is advisable. Findings have shown that a detailed magnetic behaviour study and magnetic material measurements should be conducted during development to improve efficiency and performance of electromagnetic drives. Further study should be conducted to determine the effect of nonhomogeneous eddy current distribution in laminated steel sheets on iron loss value and impact on magnetic distribution in IPM machine.

References

[1] World Permanent Magnet Motor Market – Opportunities and Forecasts, https://www.alliedmarketresearch.com/permanent-magnet-motor-market, accessed 8 August 2015.

[2] T. Finken, K. Hameyer, "Design and Optimization of an IPMSM with Fixed Outer Dimensions for Application in HEVs ", *Electric Machines and Drives Conference*, Miami, FL, May 2009, 1743–1748.

[3] A. Athavale, T. Fukushige, T. Kato, C. Yun, R. D. Lorenz, "Variable Leakage Flux (VLF) IPMSMs for Reduced Losses over a Driving Cycle while Maintaining the Feasibility of High Frequency Injection-Based Rotor Position Self-Sensing", *Energy Conversion Congress and Exposition*, Pittsburgh, PA, Sep 2014, 4523–4530.

[4] Zhiwei Zhang Libing Zhou "Design and Rotor Geometry Analysis of Permanent Magnet — Assisted Synchronous Reluctance Machines using Ferrite Magnet", *Journal of Electrical Engineering*, vol. 66, no. 6, 2015, 311–316.

[5] C. D. Graham, "Physical Origin of Losses in Conducting Ferromagnetic Materials", *Journal of Applied Physics, 1982* , vol. 53, no. 11, 8276–8280.

[6] S. Tumanski, *Handbook of Magnetic Measurements*, Boca Raton: CRC Press, 2011.

[7] G. Bertotti, "General Properties of Power Losses in Soft Ferromagnetic Materials", *IEEE Transactions on Magnetics, 1988*, vol. 24, no. 1, 621–630.

[8] T. Chevalier, A. Kedous-Lebouc, B. Cornut, C. Cester, "A New Dynamic Hysteresis Model for Electrical Steel Sheet", *Physica B: Physics of Condensed Matter, 2000*, vol. 275, no. 1-3, 197–201.

[9] J. Zhong, Y. Guo, J. Zhu, H. Lu, J. Jin, "Development of Measuring Techniques for Rotational core Losses of Soft Magnetic Materials", *Nature Sciences*, 2007, vol. 2, no. 1, 1–12.

[10] L. D. Marlino, "Report on Toyota Prius thermal management", Oak Ridge National Laboratory, 2005, 1–50.

[11] Finite Element Method Magnetics, http://www.femm.info, accessed 12 January 2015.

[12] V. GoriČan, M. Jesenik, A. Hamler, B. Štumberger, M. Trlep, "Measurement of 2-D Magnetic Properties of Grain Oriented Silicon Steel Sheet Using RRSST ", *Computer Engineering in Applied Electromagnetism*, Wiak, S., Krawczyk, A., Trlep, M., Springer Netherlands, 2005, 287–292.

[13] J. Tellinen, "A Simple Scalar Model for Magnetic Hysteresis", *IEEE Transactions on Magnetics*, 1998, vol. 34, no. 4, 2200–2206.

[14] T. Chevalier, A. Kedous-lebouc, B. Cornut, C. Cester, "Estimation of Magnetic Loss in an Induction Motor Fed with Sinusoidal Supply using a Finite Element Software and a New Approach to Dynamic Hysteresis", *IEEE Transactions on Magnetics*,1999, vol. 35, no. 5, 3400–3402.

Received 6 November 2016